

Kinematic Orienteering Problem with Time-Optimal Trajectories for Multirotor UAVs

Fabian Meyer^{1st}, fabian.meyer@fzi.de

Katharina Glock^{2nd}, kglock@fzi.de

Abstract

In many unmanned aerial vehicle (UAV) applications for surveillance and data collection, it is not possible to reach all requested locations due to the given maximum flight time. Hence, the requested locations must be prioritized and the problem of selecting the most important locations is modeled as an Orienteering Problem (OP). To fully exploit the kinematic properties of the UAV in such scenarios, we combine the OP with the generation of time-optimal trajectories with bounds on velocity and acceleration. We define the resulting problem as the Kinematic Orienteering Problem (KOP) and propose an exact mixed-integer formulation together with a Large Neighborhood Search (LNS) as a heuristic solution method. We demonstrate the effectiveness of our approach based on Orienteering instances from the literature and benchmark against optimal solutions of the Dubins Orienteering Problem (DOP) as the state-of-the-art. Additionally, we show by simulation that the resulting solutions can be tracked precisely by a modern MPC-based flight controller. Since we demonstrate that the state-of-the-art in generating time-optimal trajectories in multiple dimensions is not generally correct, we further present an improved analytical method for time-optimal trajectory generation.

Keywords: Orienteering Problem, multirotor UAV, route planning, trajectory generation, time-optimality

1 Introduction

In the last decade, UAV technology has been steadily gaining momentum. With technological advancements, UAVs are proving to be extremely useful in a variety of applications. Within this work, we focus on flight planning for surveillance and data collection, which is one of the most important use cases for UAVs [1]. In practical applications, UAVs have a limited flight time due to their battery capacity, which is why a selection of the requested locations for data collection must often be made. To do this, locations can

Original publication DOI: 10.1109/LRA.2022.3194688

©2022 IEEE. Personal use of this material is permitted. Permission from IEEE must be obtained for all other uses, in any current or future media, including reprinting/republishing this material for advertising or promotional purposes, creating new collective works, for resale or redistribution to servers or lists, or reuse of any copyrighted component of this work in other works.

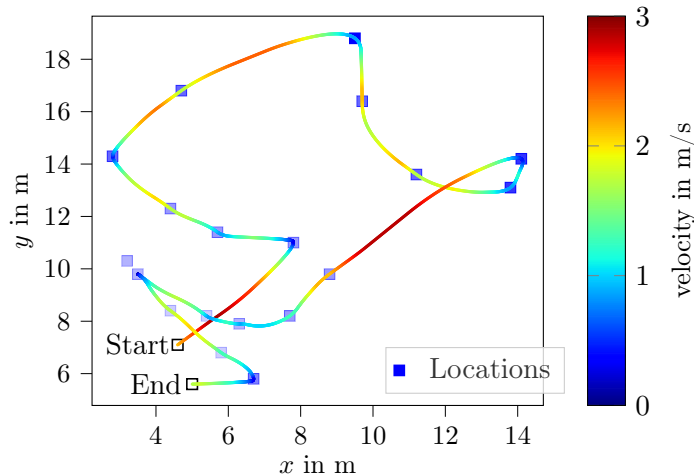


Figure 1: Example solution of the KOP for the second OP instance from Tsiligirides with bounds on the allowed acceleration $a(t) \in [-1.5, 1.5] \left(\frac{m}{s^2}\right)$ as well as bounds on the allowed velocity $v(t) \in [-3, 3] \left(\frac{m}{s}\right)$ and a maximum flight time $C_{max} = 35$ s. The changing color of the trajectory represents the corresponding velocity. The priority at each location is indicated by its opacity with a high opacity referring to a high priority.

be prioritized and the problem can be modeled as an Orienteering Problem (OP), which aims to find the trajectory that maximizes the collected priorities given the maximum flight time constraint (see [2]–[4]). For related problems, current approaches consider the UAV’s physics to generate efficient flight motions and use them as flight time estimation between locations. The most prominent examples are so-called Dubins paths and Bézier curves. Dubins paths are based on the principle of minimum turning radii, which are always feasible with regard to the underlying physics (see [1]). However, their disadvantage is that they are based on the assumption of a constant velocity. Especially for the mission planning of the widely used multirotor UAVs, the degree of freedom offered by longitudinal acceleration, which enables flying sharp turns, is thus omitted. Bézier curves, in turn, allow longitudinal acceleration. However, they do not intrinsically consider physical restrictions of the UAV such as maximum acceleration, which is why a feasible trajectory along the curve must be determined via post-processing. Furthermore, they do not provide any guarantees regarding time-efficiency.

For this reason, we propose a solution approach which is able to consider acceleration in arbitrary direction and guarantee physical feasibility as well as time-efficiency. Our approach combines the generation of time-optimal trajectories with bounds on velocity and acceleration, further denoted as kinematic trajectories, with the well-known Orienteering Problem and is therefore called Kinematic Orienteering Problem (KOP). For better understanding, Fig. 1 shows an example solution to the problem. With this work, we extend our previous research [5] and make the following contributions:

- We introduce the KOP as the problem of finding the kinematic trajectory that maximizes the collected priorities without exceeding the maximum allowed flight time.
- Further, we propose a mathematical problem formulation for the KOP and propose an easy-to-implement heuristic solution approach that yields high-quality solutions in short time.
- Additionally, we present an improved analytical approach to generate time-optimal kinematic trajectories in multiple dimensions, since we found that the state-of-the-art procedure is not generally correct.
- We benchmark our proposed solution approach against exact solution of the DOP and show by simulation that the trajectories found by our approach can precisely be tracked by a modern MPC-based flight controller.

The outline of this paper is as follows: We give an overview of related literature in Section 2. Next, we present our approach to generating time-optimal kinematic trajectories in Section 3, followed by the mathematical definition of the KOP in Section 4. Section 5 presents our heuristic solution approach and Section 6 shows the results of our approach. Finally, Section 7 concludes and gives an outlook.

2 Related Work

Since this work is, to our knowledge, the first to combine the classical Orienteering Problem, which is a subclass of route planning, with the generation of time-optimal kinematic trajectories for UAVs, this section is divided into two parts. In the first part, we give an overview of current approaches for UAV route planning. In the second part, we present the latest approaches for UAV trajectory generation.

2.1 Route Planning Problems for Multirotor UAVs

Route planning problems for multirotor UAVs are enjoying growing interest in the scientific literature. Although algorithms for solving UAV route planning problems use time-of-flight estimation based on Euclidean distances until now (see [4]) the trend has moved towards more precise and practically feasible metrics [6].

To do this, established methods include simple physical properties of UAV movements into route planning. One such characteristic is the minimum turning radius, which results from a UAV moving at constant velocity and applying maximum lateral acceleration. It is a restriction that comes

into effect especially for fixed-wing UAVs but is also considered for multi-rotor UAVs. The resulting flight paths are known as Dubins paths and are proven to be optimal regarding the assumed kinematic restrictions (see [7]). This principle is used in many UAV route planning problems. Examples include [2] and [8]. The advantage of using Dubins paths and thus assuming constant velocity is that acceleration and deceleration are avoided, making the trajectory more energy-efficient overall. Its disadvantage is that large detours may have to be accepted since the maximum acceleration has to fight against the prevailing mass inertia. At some point, these detours cancel out the efficiency advantage of a constant velocity and that is why an optimal tradeoff has to be determined [5].

Another possibility to estimate flight times for UAV route planning problems is by using so-called Bézier curves [3], [9]. Here, two locations are connected by a smooth curve based on Bernstein polynomials. By setting intermediate control points in the right way, it is possible to guide the path safely around obstacles. However, the polynomial representation of a safe path through Bézier curves is purely spatial. To ensure physical feasibility, the Bézier curve must first be transferred to the time domain. Only by assigning each spatial point of the curve to a particular point in time is it possible to consider physical constraints such as maximum velocity and acceleration (see [10]). For routing problems where thousands of trajectories are calculated this two-step procedure is computationally expensive (see [9]). Further, it is argued in [10] that if the initial and final velocity are not both zero, there may not exist a feasible solution. Moreover, another disadvantage is, especially for environments without obstacles, that the resulting trajectory is bound to the precomputed path and therefore likely to be time-suboptimal.

2.2 Trajectory Generation for Multirotor UAVs

Apart from Dubins paths and Bézier curves there are many trajectory generation approaches that plan UAV motions directly within the time domain and hence might suit better for flight time estimation. However, some of these approaches do not consider bounds on maximum velocity and acceleration either. An example is the well-known approach to generate minimum-snap trajectories, see [11], [12].

An approach that considers bounds on velocity and acceleration is model-based predictive control (MPC). It is based on a discrete-time motion model of the UAV consisting of system parameters, system state, and control variables. The objective is to find an energy-efficient sequence of control inputs that minimizes the deviation of the current state to a reference, for example, described by the desired end state, while respecting limits of control input and feasible states [13], [14]. However, MPC does not provide time-optimality, and since MPC solves a mathematical program, usually

quadratic, numerically, it is a computationally intensive method.

The last form of trajectory optimization addressed here deals with the determination of time-optimal trajectories [15], [16]. According to Pontryagin’s minimum principle (see [17]), time-optimality is achieved by having the system always operate at its physical limits. For this purpose, the overall motion of the UAV is divided into several time segments and for each, the control variable may be the maximum or the minimum control value or zero. This property is used to calculate the trajectories analytically. Further, [15] argues that time- and energy-optimality are equal in terms of the total thrust integral. Faster trajectories might consume more energy for acceleration and deceleration, but since their flight time is shorter, their energy consumption is less compared to slower trajectories.

In our previous work [5], we adapt this approach by using acceleration as control input. This enables us to generate trajectories considering fundamental physical properties and to obtain high-quality travel time estimates in a very short time. However, we found that the state-of-the-art procedure that we based our trajectory generation on is not generally correct. In Section 3, we give an example for our observation and present a refined method that solves that issue.

3 Trajectory Generation

The state-of-the-art to determine time-optimal trajectories from an arbitrary initial state to an arbitrary final state with constraints on system state and control input is based on the decoupling of axes (see [16], [18], [19]). This means that in a first step all spatial coordinate axes $i \in \{1, \dots, n\}$ of the trajectory in the n -dimensional space are separated. Pontryagin’s minimum principle is applied for each axis yielding a bang-zero-bang control input pattern. For the i -th axis with bounded acceleration as control input and a maximum allowed velocity, the resulting bang-zero-bang acceleration pattern (a_1, a_2, a_3) , which defines the acceleration profile

$$a_i(t) = \begin{cases} a_1, & 0 \leq t < t_{1,i} \\ a_2, & t_{1,i} \leq t < t_{1,i} + t_{2,i} \\ a_3, & t_{1,i} + t_{2,i} \leq t \leq t_{1,i} + t_{2,i} + t_{3,i} = t_e, \end{cases}$$

is given by $(+a, 0, -a)$ with either $a = -a_{max}$ or $a = +a_{max}$ and a_{max} representing the maximum allowed acceleration. The durations of each time segment of constant acceleration are described by $t_{1,i}, t_{2,i}$ and $t_{3,i}$. In case the velocity limit is not reached, $t_{2,i} = 0$ holds. Consequently, the time-optimal trajectory consists of two time segments of constant maximum acceleration with opposite sign and, if the velocity limit is reached, one segment of no acceleration. The time-optimal trajectory duration $T_{opt,i}$ can be calculated

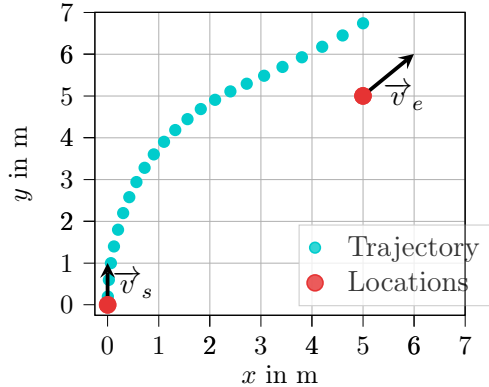


Figure 2: Example for insynchronizability of a given initial and end state.

analytically (e.g. see [5]). Next, the state-of-the-art postulates that the overall duration T_{sync} is defined as the largest of the time-optimal durations $T_{opt,i}$ over all axes, i.e.

$$T_{sync} = \max_{i \in \{1, \dots, n\}} \{T_{opt,i}\}. \quad (1)$$

However, this procedure sometimes results in unexpected behavior since not all axes can be synchronized with the duration T_{sync} . The reason is that this approach does not consider the inertia of the movement properly, and therefore, sometimes results in overshooting the desired final state. This effect has not been reported in the literature so far. Next, we give an example where this approach is invalid.

Figure 2 illustrates the trajectory generation in two dimensions x and y based on the state-of-the-art. For the x axis the initial state is $p_{x,s} = 0$ m, $v_{x,s} = 0 \frac{\text{m}}{\text{s}}$, where $p_{x,s}$ describes the initial position and $v_{x,s}$ the initial velocity. The desired end state for the x axis is $p_{x,e} = 5$ m, $v_{x,e} = 2 \frac{\text{m}}{\text{s}}$. The time-optimal duration for a maximum allowed acceleration $a \in [-0.5, 0.5] (\frac{\text{m}}{\text{s}^2})$ and velocity $v \in [-2, 2] (\frac{\text{m}}{\text{s}})$ can be calculated as described in [5] and is $T_{opt,x} = 4.5$ s. For the y axis the initial and end state are $p_{y,s} = 0$ m, $v_{y,s} = 2 \frac{\text{m}}{\text{s}}$, $p_{y,e} = 5$ m, $v_{y,e} = 2 \frac{\text{m}}{\text{s}}$. Here, the calculation of the time-optimal duration yields $T_{opt,y} = 2.5$ s. According to Equation (1), both axes must be synchronized at $T_{sync} = 4.5$ s. By utilizing MPC for trajectory synchronization with a fixed duration, it can be seen that the resulting two dimensional trajectory (blue dots in Figure 2) misses the required end state by far. This behavior is due to the inertia of the system. The high initial velocity along the y axis in combination with an insufficient acceleration power leads to overshooting the end position $p_{y,e}$. As a result, although the y axis has the potentially faster execution, it cannot be synchronized with the slower time-optimal duration of the x axis.

For the above scenario, Figure 3 shows feasible velocity profiles for different synchronization times T_{sync} for the y axis with respect to the desired end

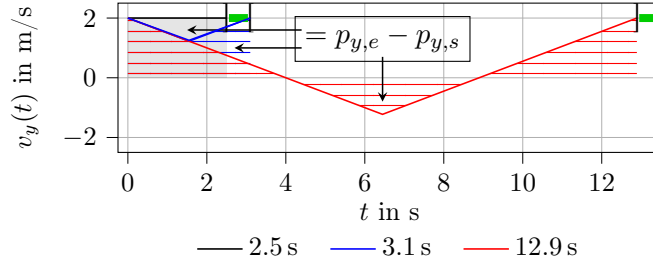


Figure 3: Range of valid trajectory durations shown in green. The velocity profiles that lead to the limits of the corresponding range are given by colored lines. The associated areas underneath these profiles are highlighted in the respective colors.

state. The property of a feasible trajectory is that the desired start and end velocity must be achieved, and the integral underneath the velocity profile must equal $p_{y,e} - p_{y,s}$. The velocity profile $v_y(t)$ of the time-optimal trajectory is shown by a solid black line. Since its initial velocity already equals the maximum allowed value, it remains constant and $T_y = T_{opt,y} = 2.5$ s results. If it is required to increase the trajectory duration, i.e. $T_y > 2.5$ s, the UAV first decelerates the motion and accelerates afterwards to meet the required final velocity $v_{y,e} = 2 \frac{\text{m}}{\text{s}}$. However, this procedure works only as long as the integral underneath the velocity profile equals $p_{y,e} - p_{y,s}$. The slowest velocity profile that does not violate this condition corresponds to $T_y \approx 3.1$ s (see blue line). Further increasing the required trajectory duration leads to overshooting until $T_y \geq 12.9$ s (see red line). From this duration on it is possible to compensate for overshooting by flying a turn. In total, the range of feasible trajectory durations with respect to the requirements on the y axis is given in green. As can be seen, a synchronization with $T_{sync} = T_{opt,x} = 4.5$ s is not possible.

In the following, we show our general approach to design time-optimal trajectories for multiple axes. First, we present acceleration patterns needed for our approach and discuss how we can check whether these patterns can be synchronized with a particular trajectory duration T_{sync} . Second, we describe a general procedure to obtain the time-optimal duration.

3.1 Synchronization Feasibility

In this subsection, we only focus on the feasibility of synchronizing a single axis with a particular T_{sync} , and therefore the subscript i will be discarded. To check feasibility, we first define the considered acceleration patterns. On the one hand, we consider the acceleration patterns for time-optimality in a single axis given by $(+a, 0, -a)$ with $a \in \{-a_{max}, a_{max}\}$. These patterns are from now on called classical patterns. However, we further consider the patterns defined by $(+a, 0, +a)$ with $a \in \{-a_{max}, a_{max}\}$, which we denote as synchronization patterns. The reason for the latter is that classical patterns aim at finding the time-optimal behavior, however, they are not sufficient in

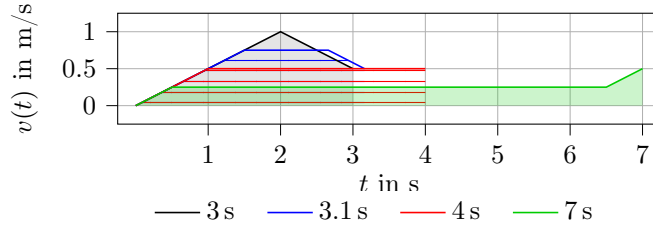


Figure 4: Example of velocity profiles for different acceleration patterns and trajectory durations.

some cases of synchronization with large synchronization times. We give the following example for illustration (see Figure 4): It is assumed that an axis with $p_s = 0\text{ m}$, $p_e = 1.75\text{ m}$ and $v_s = 0\frac{\text{m}}{\text{s}}$, $v_e = 0.5\frac{\text{m}}{\text{s}}$ has to be synchronized with a large enough duration T_{sync} . Here, p_s , p_e , v_s and v_e describe initial and end position as well as velocity.

The pattern yielding time-optimality is given by $(+a_{max}, 0, -a_{max})$, with the black line giving the overall time-optimal velocity profile. However, this pattern is only applicable as long as $T_{sync} \leq 4\text{ s}$. When T_{sync} is increased, the segment of deceleration at the end of the velocity profile shortens in time (blue line) until it becomes zero for synchronization time $T_{sync} = 4$ (red line). If it is required to synchronize the axis with $T_{sync} > 4\text{ s}$ using the classical pattern $(+a_{max}, 0, -a_{max})$, no solution can be found anymore since it is not possible to meet the desired final velocity and area underneath the velocity profile at the same time. In this case, the synchronization patterns $(+a, 0, +a)$, $a \in \{-a_{max}, a_{max}\}$ with two phases of acceleration pointing towards the same direction come into play (green line). With such a pattern it is possible to synchronize the axis with $T_{sync} > 4\text{ s}$. We define these patterns as synchronization patterns because they are only needed for axis synchronization.

To guarantee synchronization feasibility of one axis with the trajectory time T_{sync} , one has to find a pattern from the set of classical and synchronization patterns where $t_1, t_2, t_3 \geq 0\text{ s}$ and $v_{min} \leq v(t) \leq v_{max}, \forall t \in [0, T_{sync}]$. We define these inequations as synchronization conditions. Note that, if the initial and end velocities v_s and v_e are within the velocity bounds, it is sufficient to show that the constant velocity $v_c = v(t_1)$ in the segment of no acceleration is within the velocity bound to guarantee that $v_{min} \leq v(t) \leq v_{max}$. The following subsections present how the values t_1, t_2, t_3, v_c are determined for classical and synchronization patterns.

3.1.1 Classical Patterns

The classical patterns are defined by the acceleration profile

$$a(t) = \begin{cases} +a, & 0 \leq t < t_1 \\ 0, & t_1 \leq t < t_1 + t_2 \\ -a, & t_1 + t_2 \leq t \leq t_1 + t_2 + t_3. \end{cases} \quad (2)$$

with $a \in \{a_{max}, -a_{max}\}$. Based on this acceleration profile, the velocity profile results in

$$v(t) = \begin{cases} v_s + at, & 0 \leq t < t_1 \\ v_s + at_1, & t_1 \leq t < t_1 + t_2 \\ v_s + 2at_1 - a(t - t_2) & t_1 + t_2 \leq t \leq t_1 + t_2 + t_3 \end{cases} \quad (3)$$

In order to meet the required velocity v_e at time $t_1 + t_2 + t_3$ the following equation has to hold:

$$\begin{aligned} v_e - v_s &= \int_0^{t_1+t_2+t_3} a(t)dt \\ &= at_1 - at_3 \end{aligned} \quad (4)$$

To meet the required position p_e at time $t_1 + t_2 + t_3$ the equation

$$\begin{aligned} p_e - p_s &= \int_0^{t_1+t_2+t_3} v(t)dt \\ &= v_s t_1 + \frac{1}{2}at_1^2 + (v_s + at_1)t_2 + (v_s + at_1)t_3 - \frac{1}{2}at_3^2 \end{aligned} \quad (5)$$

has to hold as well. Additionally, the equation

$$t_1 + t_2 + t_3 = T_{sync} \quad (6)$$

has to hold to guarantee time synchronization. Further, since the velocity v_c for $t \in [t_1, t_2]$ is constant, the equation

$$v_c = at_1 + v_s \quad (7)$$

applies as well.

Equations (4), (5), (6) and (7) form a system of equations with variables t_1, t_2, t_3, v_c whose solution is given by

$$t_1 = \frac{aT_{sync} + v_e - v_s \pm \sqrt{A}}{2a} \quad (8)$$

$$t_2 = \mp \frac{\sqrt{A}}{a} \quad (9)$$

$$t_3 = \frac{aT_{sync} - v_e + v_s \pm \sqrt{A}}{2a} \quad (10)$$

$$v_c = \frac{aT_{sync} + v_s + v_e + \sqrt{A}}{2} \quad (11)$$

with

$$A = a^2 T_{sync}^2 + 2(v_e + v_s)aT_{sync} - 4a(x_e - x_s) - (v_e - v_s)^2. \quad (12)$$

Equations (8), (9), (10) and (11) only depend on the trajectory duration T_{sync} . Hence, it is sufficient to insert T_{sync} into these equations and verify that $t_1(T_{sync}), t_2(T_{sync}), t_3(T_{sync}) \geq 0$ and $v_{min} \leq v_c(T_{sync}) \leq v_{max}$ to show synchronization feasibility for the respective classical pattern.

3.1.2 Synchronization Patterns

Synchronization feasibility for the synchronization patterns is checked analogously. The only difference is in the applied acceleration pattern

$$a(t) = \begin{cases} +a, & 0 \leq t < t_1 \\ 0, & t_1 \leq t < t_1 + t_2 \\ +a, & t_1 + t_2 \leq t \leq t_1 + t_2 + t_3 \end{cases} \quad (13)$$

with $a \in \{a_{max}, -a_{max}\}$, which results in the following velocity profile

$$v(t) = \begin{cases} v_s + at, & 0 \leq t < t_1 \\ v_s + at_1, & t_1 \leq t < t_1 + t_2 \\ v_s + a(t - t_2) & t_1 + t_2 \leq t \leq t_1 + t_2 + t_3 \end{cases} \quad (14)$$

Analogously, this leads to a system of four equations and four variables whose solution is given by

$$t_1 = \frac{(-2v_s T_{sync} + 2(p_e - p_s))a - (v_e - v_s)^2}{2a(T_{sync}a - v_e + v_s)} \quad (15)$$

$$t_2 = \frac{aT_{sync} - v_e + v_s}{a} \quad (16)$$

$$t_3 = \frac{(-2v_e T_{sync} - 2(p_e - p_s))a - (v_e - v_s)^2}{2a(T_{sync}a - v_e + v_s)} \quad (17)$$

$$v_c = \frac{2a(p_e - p_s) - v_e^2 + v_s^2}{2(aT_{sync} - v_e + v_s)} \quad (18)$$

Again, equations (15), (16), (17) and (18) only depend on T_{sync} and the synchronization conditions can easily be checked via insertion.

3.2 Optimal Synchronization Time

In this subsection, we show how to find the time-optimal duration for multiple axes. The set of valid synchronization times Ω is continuous and constrained by the synchronization conditions. To find the time-optimal duration for multiple axes, one has to investigate the boundary of Ω . This is

where $t_1, t_2, t_3 \geq 0$ as well as $v_c \geq v_{min}$ and $v_c \leq v_{max}$ holds and at least one of these inequalities is fulfilled with equality. Hence, each T_{sync} that fulfills equality for any of the synchronization conditions is a potential candidate for the time-optimal duration for multiple axes. To determine the best synchronization time for multiple axes, all candidates $T_{sync} \geq \max_{i \in \{1, \dots, n\}} \{T_{opt,i}\}$, with $T_{opt,i}$ for the i -th axis calculated as described in [5], are inserted into the synchronization conditions of each axis and pattern and checked for feasibility. The lowest trajectory synchronization time that yields feasibility for at least one pattern in each axis is defined as the optimal synchronization time T^* . With the associated values t_1, t_2, t_3 for the corresponding patterns it is possible to reconstruct the trajectory.

4 Kinematic Orienteering Problem

The objective of the KOP is to find the kinematic trajectory through a set of locations that maximizes the sum of priorities of the selected locations while considering the maximum flight time. The proposed mathematical optimization model for the KOP assumes that a UAV can move through a location with a discretized heading angle and additionally at a discretized velocity. As a generalization of the OP, the KOP is also NP-hard (see [20]).

4.1 Assumptions and Notations

We solve the KOP for multirotor UAVs in an obstacle-free two-dimensional plane where each element in a set of locations $\mathcal{L} = \{l_i : i = 1, \dots, L\}$ can be traversed with discretized heading angle and with a discretized velocity and is assigned a priority $r_i \in \mathbb{R}_0^+$. Start and end locations are represented by l_1 and l_L . The two-dimensional case is addressed, since it is the basis of an extension into the three-dimensional space and to enable a direct comparison to the Dubins Orienteering Problem (DOP) as state-of-the-art on benchmark instances.

With H and V representing the number of discretization levels for heading angles and velocities, we define the set of discretized heading angles as $\mathcal{H} = \{h_i : h_i = 2\pi i/H, i = 1, \dots, H\}$. The set of discretized velocities depends on the maximum allowed velocity and consists of elements $\mathcal{V} = \{v_i : v_i = (i - 1)v_{max}/(V - 1), i = 1, \dots, V\}$.

Costs that describe the flight time to get from location l_i with heading angle h_k and velocity v_g to location l_j with heading angle h_m and velocity v_w are defined by c_{ikg}^{jmw} and are determined by our trajectory generation method presented above. The maximum flight time is denoted as C_{max} .

4.2 Mathematical Formulation of the KOP

The mathematical programming formulation to determine the priority-maximizing sequence of locations, as well as the corresponding heading angles and velocity configurations that define the UAV's trajectory, is presented in the following.

The main decision variables for our formulation x_{ikg}^{jmw} are binary and interpreted as

$$x_{ikg}^{jmw} = \begin{cases} 1, & \text{if location } l_i \text{ is left with heading angle } h_k \\ & \text{and velocity } v_g \text{ towards location } l_j, \text{ which is} \\ & \text{entered with heading angle } h_m \text{ and velocity } v_w, \\ 0, & \text{otherwise} \end{cases}$$

Furthermore, integer decision variables $u_i \in \{1, \dots, L\}, i = 1, \dots, L$ define the sequence of visited locations l_i in the tour. The overall KOP model is given as follows.

$$\max \sum_{i=2}^{L-1} \sum_{j=2}^L \sum_{k=1}^H \sum_{m=1}^H \sum_{g=1}^V \sum_{w=1}^V x_{ikg}^{jmw} r_j \quad (19)$$

s.t.

$$\sum_{j=2}^L \sum_{k=1}^H \sum_{m=1}^H \sum_{g=1}^V \sum_{w=1}^V x_{1kg}^{jmw} = 1 \quad (20)$$

$$\sum_{i=1}^{L-1} \sum_{k=1}^H \sum_{m=1}^H \sum_{g=1}^V \sum_{w=1}^V x_{ikg}^{Lmw} = 1 \quad (21)$$

$$\sum_{i=1}^{L-1} \sum_{k=1}^H \sum_{m=1}^H \sum_{g=1}^V \sum_{w=1}^V x_{ikg}^{jmw} \leq 1 \quad \forall j = 2, \dots, L \quad (22)$$

$$\sum_{i=1}^{L-1} \sum_{k=1}^H \sum_{g=1}^V x_{ikg}^{jmw} = \sum_{o=2}^L \sum_{p=1}^H \sum_{q=1}^V x_{jpm}^{opq} \quad \forall j = 2, \dots, L-1$$

$$\forall m = 1, \dots, H$$

$$\forall w = 1, \dots, V \quad (23)$$

$$\sum_{i=1}^{L-1} \sum_{j=2}^L \sum_{k=1}^H \sum_{m=1}^H \sum_{g=1}^V \sum_{w=1}^V x_{ikg}^{jmw} c_{ikg}^{jmw} \leq C_{max} \quad (24)$$

$$(25)$$

$$u_i - u_j + 1 \leq (L - 1) \left(1 - \sum_{k=1}^H \sum_{m=1}^H \sum_{g=1}^V \sum_{w=1}^V x_{ikg}^{jmw} \right) \quad \forall i, j = 1, \dots, L \quad (26)$$

$$u_1 = 1 \quad (27)$$

$$u_i \in \{2, \dots, L\} \quad \forall i = 2, \dots, L \quad (28)$$

$$x_{ikg}^{jmw} \in \{0, 1\} \quad \forall i, j = 1, \dots, L$$

$$\quad \forall k, m = 1, \dots, H$$

$$\quad \forall g, w = 1, \dots, V \quad (29)$$

The objective of the presented mathematical programming formulation (19) is to maximize the collected priorities. Constraint (20) enforces that the start location is left whereas constraint (21) enforces that the end location is entered. Constraint set (22) ensures that each location is entered at most once. Flow conservation is fulfilled by constraint set (23). These constraints ensure that location l_j is left in the same direction as it is entered as well as with the same velocity. Constraints (24) ensure that the maximum allowed flight time is not exceeded. To prevent subtours, we make use of the subtour elimination constraints (26), (27) and (28) which are formulated according to the Miller-Tucker-Zemlin (MTZ) formulation [21]. Constraints (29) enforce the decision variable x_{ikg}^{jmw} to be binary.

5 Heuristic Solution Approach

For larger problem instances, the KOP is too complex to be solved exactly. Therefore, we propose a heuristic solution approach based on a Large Neighborhood Search (LNS) framework, which is a widely used and easy-to-implement approach for route planning problems [22]. Starting from an initial solution generated by a construction heuristic, we iteratively destroy 50% of the solution and then apply the construction heuristic again. After 100 iterations, we use the best-found solution as a new initial solution for the same procedure for another 100 iterations but destroy only 20% of the solution. The objective is to search for good solutions globally in the first step, and in the second step, we are locally optimizing the best-found solution so far. In the following, we present the applied construction and the destruction heuristics.

5.1 Construction Heuristic

We propose a construction heuristic that inserts unscheduled locations l_p into an existing plan by evaluating the ratio of potentially collected priority r_p and additional flight time used for insertion. Since a location l_p can be

traversed in multiple ways according to heading angle h_p and velocity v_p , we only consider the best insertion possibility, i.e. where the additional flight time is minimal:

$$c_{i,p,j}^* := \min_{h_p \in \mathcal{H}, v_p \in \mathcal{V}} c_{i,h_i,v_i}^{p,h_p,v_p} + c_{p,h_p,v_p}^{j,h_j,v_j} - c_{i,h_i,v_i}^{j,h_j,v_j}$$

In this term, i and j refer to the predecessor and successor locations l_i and l_j of location l_p . At this point, heading angles and velocities at the predecessor and successor are fixed. Hence, the term describes the additional costs of inserting location l_p with optimal heading angle h_p and velocity v_p in between l_i and l_j . The best insertion for location l_p in between any predecessor l_i and successor l_j is associated with the highest ratio

$$\mathcal{R}_p^* = r_p \left[\min_{i,j} c_{i,p,j}^* \right]^{-1}.$$

This is done for all unscheduled locations. The insertion with the overall highest ratio is realized. The construction heuristic terminates when no further insertion is possible without violating the maximum flight time restriction. As post-processing for each insertion, we optimize the heading angle and velocity of the start and end location.

5.2 Destruction Heuristics

To destroy a part of the incumbent solution, we make use of three different destruction heuristics, which are applied randomly until the predefined percentage of destruction is reached. The first heuristic removes the location from the existing solution whose ratio between gained priority and flight time used is the lowest. As a second destruction heuristic, we remove the location whose assigned heading angle and velocity do not connect it with its predecessor and successor optimally. This is checked via full enumeration. The third heuristic combines both and removes the location whose ratio between the gained priority and the difference between current flight time and best possible flight time is the lowest.

6 Results

To evaluate our LNS solution approach and the benefit of the KOP formulation, we generate globally optimal benchmark solutions of the Dubins Orienteering Problem (DOP) and compare them to exact and heuristic solutions of the KOP. Moreover, we show that the yielded solutions can be used as reference trajectories for multirotors since we demonstrate that they can precisely be tracked by a modern MPC-based flight controller.

6.1 Benchmark against DOP

We generate benchmarks on Tsiligirides dataset 2 (see [23]) with slightly modified time budget constraints to be more representative. We chose dataset 2 since it is the only OP dataset whose problem instances could be solved with Gurobi as a commercial solver to optimality within a reasonable time. The kinematic properties we assume for the evaluation are $v_{max} = 3 \frac{\text{m}}{\text{s}}$ and $a_{max} = 1.5 \frac{\text{m}}{\text{s}^2}$. Further, we assume that each waypoint can be traversed with eight different and equally distributed heading angles. To determine the optimal solutions for the DOP, we calculate Dubins paths and used their length divided by the constant velocity as edge costs. Dubins paths require a minimum turning radius as input which results from the centripetal force and is calculated by $r = v_{const}^2 / a_{max}$. Since a_{max} is a physically given and UAV-specific constant the turning radius can only be changed by a modification of v_{const} . However, decreasing the constant velocity to achieve short paths might result in higher flight times.

To find the best instance dependent constant velocity, we solved the DOP for each constant velocity $v_{const} \in \{0.1, 0.2, \dots, 1.0\} \cdot v_{max}$. The highest collected priorities for the different maximum allowed flight times C_{max} over all v_{const} are presented in the second column of Table 1. To directly benchmark the KOP-formulation with the DOP-formulation, we solve the corresponding KOPs with $V = 1$ to optimality by using the associated v_{const} scaled by $\sqrt{2}^{-1}$ as traversal velocities. The scaling is applied to not exceed the maximum allowed velocity of a single axis, which must be bounded to $[-3, 3] \cdot \frac{1}{\sqrt{2}} \left(\frac{\text{m}}{\text{s}}\right)$ to guarantee that the total maximum velocity is not exceeded and hence to be comparable with the DOP. For the same reason, the bound on maximum allowed acceleration for each axis in our trajectory generation is scaled with $\sqrt{2}^{-1}$ as well. The results are given in the third column of Table 1 (KOP-1*). It can be seen that the optimal solution of the KOP constantly collects approximately 20% more priorities than the best possible solution of the DOP for all instances. Note that the overall highest collected priorities are marked bold in Table 1.

To demonstrate the effectiveness of the proposed LNS, we again conduct the same procedure for the KOP with our heuristic solution approach as solver. For each problem instance and each traversal velocity, we conducted ten runs, each with a different random seed. The overall highest collected priorities and the average collected priorities for the associated traversal velocity in brackets, demonstrating the competitiveness with the exact approach, are given in the fourth column of Table 1.

Lastly, we solved the KOP as modeled in Section 4 with multiple options for traversal velocities. In the first case (KOP-3^{LNS}), we consider the set of allowed velocities to be $\mathcal{V} = \{0, 0.5, 1\} \cdot v_{max} / \sqrt{2}$. In the second case (KOP-6^{LNS}), $\mathcal{V} = \{0, 0.2, 0.4, 0.6, 0.8, 1\} \cdot v_{max} / \sqrt{2}$ holds. Table 1 shows that for many problem instances the LNS approach yields even better solutions

C_{max}	Best fixed traversal velocity			Varying traversal velocity	
	DOP*	KOP-1*	KOP-1 ^{LNS}	KOP-3 ^{LNS}	KOP-6 ^{LNS}
10 s	80	95	80 (80)	70 (70)	80 (75)
15 s	155	180	180 (153)	175 (170)	165 (165)
20 s	215	250	235 (225)	230 (226.5)	250 (237.5)
25 s	275	325	315 (295.2)	330 (311.5)	330 (316.5)
30 s	315	390	390 (367.5)	385 (369.5)	390 (377.5)
35 s	370	430	425 (411.5)	430 (415)	435 (422.5)
40 s	415	450	450 (447)	450 (446)	450 (450)

Table 1: Results for each solution method Tsiligirides dataset 2 containing 21 locations. The asterisk as superscript denotes that the problem instances were solved exactly, whereas LNS indicates the application of our heuristic solver. Average collected priorities for our LNS approach are given in brackets.

than found by the exact approach (KOP-1*). This is possible since a higher degree of freedom for the traversal velocity is offered, which can successfully be exploited. However, for $C_{max} = 10$ no improvements compared to the optimal DOP solutions can be found. Sometimes the solution is even worse than the optimal DOP solution. We assume this to be the case since the velocity yielding the best solution for KOP-1* is not considered. To illustrate the resulting trajectories, an example solution for $V = 6$ and $H = 8$ is given in Fig. 1. The efficiency of the trajectory is clearly visible since slow velocities only occur when sharp turns are required.

Our exact approach, LNS and the trajectory generation are implemented in Python and executed on an Intel Core i7-8565U CPU. The average computation time of a single trajectory is 62 μ s. The average runtimes for each solution method are presented in a logarithmic scale in Figure 5. Some problem instances for the DOP* and KOP-1* could not even be solved to optimality within a runtime of 100.000 s. In these cases, we set the average runtime for the ten different traversal velocities to be greater than 10.000 s. Nevertheless, since the dual bounds for the suboptimal solutions provided by Gurobi are worse than the proven optimal solutions for other traversal velocities, the optimality of the values presented in Table 1 holds. Contrary to the exact approaches, the LNS finds high-quality solutions in a short time and with slowly increasing runtimes for increasing problem sizes. Therefore, we see the benefit of our heuristic solution approach when it comes to larger problem instances.

6.2 Trackability of Solutions

We simulatively indicate the precise trackability of the solutions by the utilization of a modern MPC-based UAV trajectory tracking controller. For that, we apply a twelve state dynamic quadrotor model from [24] with squared angular velocity for each rotor as the control input to represent

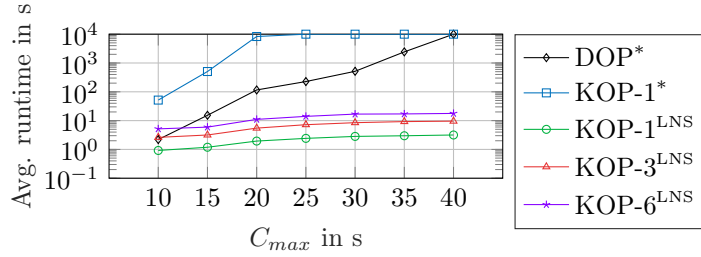


Figure 5: Average runtimes for each solution approach over all problem instances for a specific C_{max} .

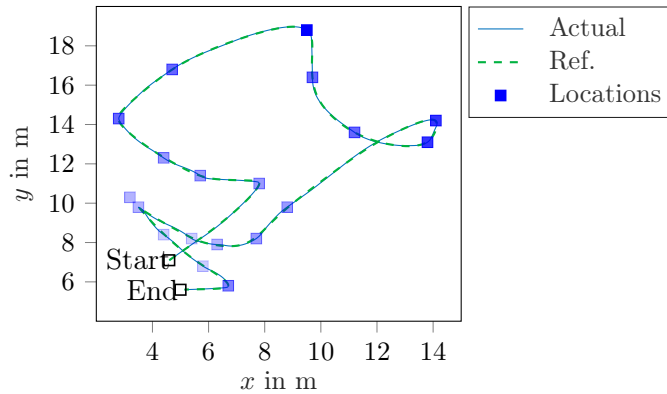


Figure 6: Plot of the actual and the reference position for the solution of Tsiligirides problem instance number two with $C_{max} = 35$ s.

real dynamic behavior. Next, we apply a nonlinear MPC according to [25], which is provided by the MPC toolbox in MATLAB, with a sampling time of 0.1 s and a prediction horizon of 1.8 s. We use the position of the trajectory shown in Figure 1 as a reference for demonstration. Figure 6 shows that the reference trajectory is tracked precisely with neglectable overshoots in position due to the deviation between the kinematic model for generating the reference trajectory and the nonlinear dynamic quadrotor model representing real behavior. The tracking error for the position and as well as the actual velocity and acceleration profile are given in blue in Figure 7, whereas the solution of the KOP as reference is given in green. The root mean square error (RMSE) of the obtained trajectory compared with the reference trajectory is 0.035 m. It can be seen that the velocity and acceleration profiles of the reference exactly comply with the predefined bounds. The same holds for the actual trajectory with a few minor exceptions for the control inputs, since the applied MPC has constraints on the maximum thrust but not on the maximum acceleration.

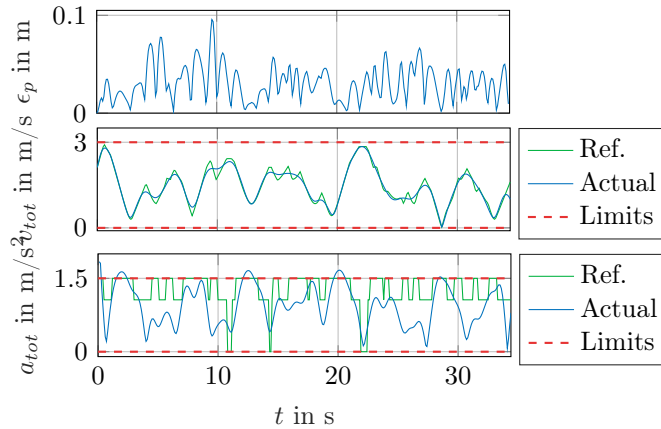


Figure 7: Position error ϵ_p , total velocity v_{tot} and total acceleration a_{tot} (with limits) for tracking the reference trajectory shown in Figure 6.

7 Conclusion and Outlook

In this work, we define the Kinematic Orienteering Problem and benchmark exact and heuristically obtained solutions against optimal solutions of the DOP. For flight time estimation, we present an improved analytical approach to calculate time-optimal multidimensional trajectories with bounded acceleration and velocity and demonstrate why the state-of-the-art approach is not valid in general. Further, we show that the obtained overall trajectories can precisely be tracked by a modern MPC-based UAV flight controller. To our knowledge, this constitutes the first approach that enables time-optimal mission planning for multirotor UAVs with consideration of their full physical capabilities. In future work, we will improve the computational performance and quality of our heuristic solution approach and investigate the KOP in three-dimensional scenarios.

References

- [1] A. Otto, N. Agatz, J. Campbell, B. Golden, and E. Pesch, “Optimization approaches for civil applications of unmanned aerial vehicles (UAVs) or aerial drones: A survey,” *Networks*, vol. 72, pp. 411–458, 2018.
- [2] R. Penicka, J. Faigl, P. Vana, and S. M., “Dubins orienteering problem,” *IEEE Robotics and Automation Letters*, vol. 2, pp. 1210–1217, 2017.
- [3] J. Faigl, P. Vana, and R. Penicka, “Multi-vehicle close enough orienteering problem with Bézier curves for multi-rotor aerial vehicles,” *International Conference on Robotics and Automation*, 2019.
- [4] E. Fountoulakis, G. S. Paschos, and N. Pappas, “UAV trajectory optimization for time constrained applications,” *IEEE Networking Letters*, vol. 2, no. 3, pp. 136–139, 2020.

- [5] F. Meyer and K. Glock, "Trajectory-based Traveling Salesman Problem for multirotor UAVs," *International Conference on Distributed Computing in Sensor Systems*, 2021.
- [6] M. Henchey and S. Rosen, "Emerging approaches to support dynamic mission planning: Survey and recommendations for future research," *Journal of Defense Modelling and Simulation: Applications, Methodology, Technology*, 2020.
- [7] L. E. Dubins, "On curves of minimal length with a constraint on average curvature, and with prescribed initial and terminal positions and tangents," *American Journal of Mathematics*, vol. 79, no. 3, pp. 497–516, 1957.
- [8] K. Sundar, S. Sanjeevi, and C. Montez, "A branch-and-price algorithm for a team orienteering problem with fixed-wing drones," *EURO Journal on Transportation and Logistics*, vol. 11, p. 100 070, 2022.
- [9] J. Faigl and P. Vana, "Surveillance planning with Bézier curves," *IEEE Robotics and Automation Letters*, vol. 3, no. 2, pp. 750–757, 2019.
- [10] F. Gao, W. Wu, J. Pan, B. Zhou, and S. Shen, "Optimal time allocation for quadrotor trajectory generation," *International Conference on Intelligent Robots and Systems (IROS)*, 2018.
- [11] D. Mellinger and V. Kumar, "Minimum snap trajectory generation and control for quadrotors," *IEEE International Conference on Robotics and Automation*, 2011.
- [12] R. Charles, A. Bry, and N. Roy, "Polynomial trajectory planning for aggressive quadrotor flight in dense indoor environments," *Robotic Research*, pp. 649–666, 2016.
- [13] M. W. Mueller and R. D'Andrea, "A model predictive controller for quadrotor state interception," *European Control Conference*, 2013.
- [14] M. Kamel, T. Stastny, K. Alexis, and R. Siegward, "Model predictive control for trajectory tracking of unmanned aerial vehicles using robot operating system," in *Robot Operating System (ROS): The Complete Reference (Volume 2)*, A. Koubaa, Ed. Springer International Publishing, 2017, pp. 3–39.
- [15] M. Beul and S. Behnke, "Analytical time-optimal trajectory generation and control for multirotors," *International Conference on Unmanned Aircraft Systems (ICUAS)*, 2016.
- [16] M. Beul and S. Behnke, "Fast full state trajectory generation for multirotors," *International Conference on Unmanned Aircraft Systems (ICUAS)*, 2017.
- [17] L. Pontryagin, *Mathematical Theory of Optimal Processes*. Taylor & Francis, 1987.
- [18] M. W. Mueller, M. Hehn, and R. D'Andrea, "A computationally efficient algorithm for state-to-state quadrotor trajectory generation and feasibility verification," *International Conference on Intelligent Robots and Systems (IROS)*, 2013.
- [19] M. Hehn and R. D'Andrea, "Real-time trajectory generation for quadrotors," *IEEE Transactions on Robotics*, vol. 31, pp. 877–892, 4 2015.
- [20] B. Golden, L. Levy, and R. Vohra, "The orienteering problem," *Naval Research Logistics*, vol. 34, "307–318, 1987.
- [21] C. E. Miller, A. W. Tucker, and R. A. Zemlin, "Integer programming formulation of Traveling Salesman Problems," *Journal of the ACM*, vol. 7, pp. 326–329, 1960.
- [22] D. Pisinger and S. Ropke, "Large Neighborhood Search," in *Handbook of Metaheuristics*, M. Gendreau and J.-Y. Potvin, Eds. Springer International Publishing, 2018, pp. 99–127.
- [23] T. Tsiligirides, "Heuristic methods applied to orienteering," *J. Oper. Res. Soc.*, vol. 35, no. 9, pp. 797–809, 1984.

- [24] T. Luukkonen, “Modelling and control of quadcopter,” *Independent research project in applied mathematics*, Espoo: *Alto University*, 2011.
- [25] E. Tzorakoleftherakis and T. D. Murphey, “Iterative sequential action control for stable, model-based control of nonlinear systems,” *IEEE Transactions on Automatic Control*, 2018.